Supplemental Figures:

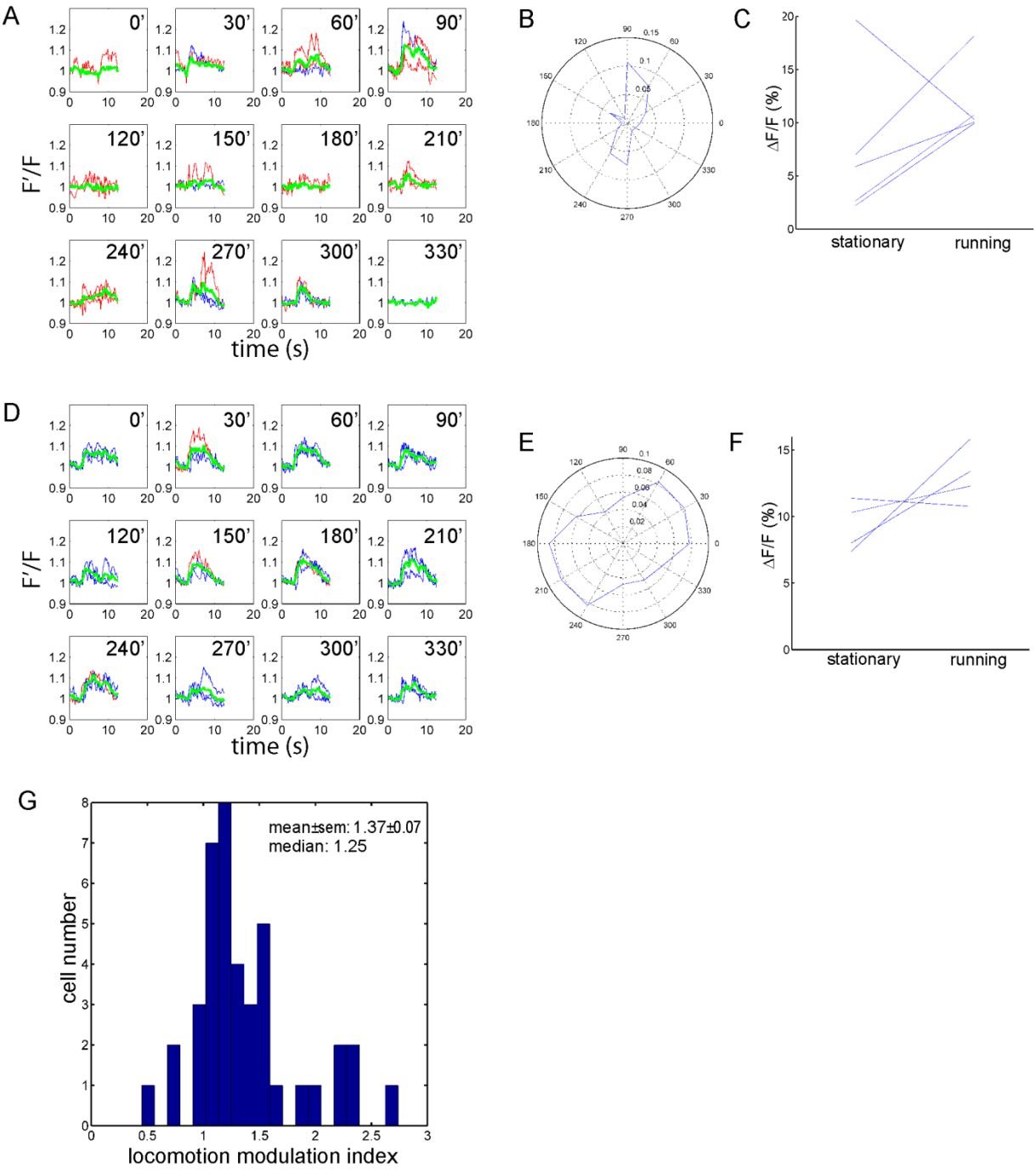

Supplemental Figure 1. Enhancement of visual response by locomotion measured using calcium imaging *in vivo*. Related to Figure 1. (A) V1 was loaded with OGB-1 in VIP-Cre:Ai14 mouse

that was free to run on a Styrofoam ball floating on air. The calcium responses of a non-VIP neuron to drifting gratings moving in different directions when the animal was stationary shown in blue and during locomotion shown in red (in each case responses shown only when the response amplitude was bigger than 3 times of the SD of the first 1 sec baseline level); green traces show the average of all the responses regardless of the response amplitude. (B) Polar chart of the averaged responses in (A), showing this neuron was narrowly tuned for stimulus orientation. (C) For each direction where there were both red traces and blue traces (meaning significant responses under both conditions), the running response computed as the average of the red traces is connected by a thin line to the stationary response computed as the average of the blue traces. (D-F) An example of the broadly tuned neuron, illustrated as described in (A-C). (E) Histogram of the distribution of the locomotion modulation index of all the non-VIP neurons. (G) For each direction where there were both red traces and blue traces (meaning significant responses under both conditions), the running response computed as the average of the red traces was divided by the stationary response computed as the average of the blue traces to derive a 'locomotion modulation value' for that direction. By averaging all the 'locomotion modulation values' for different directions, we compute a 'locomotion modulation index' for each neuron.

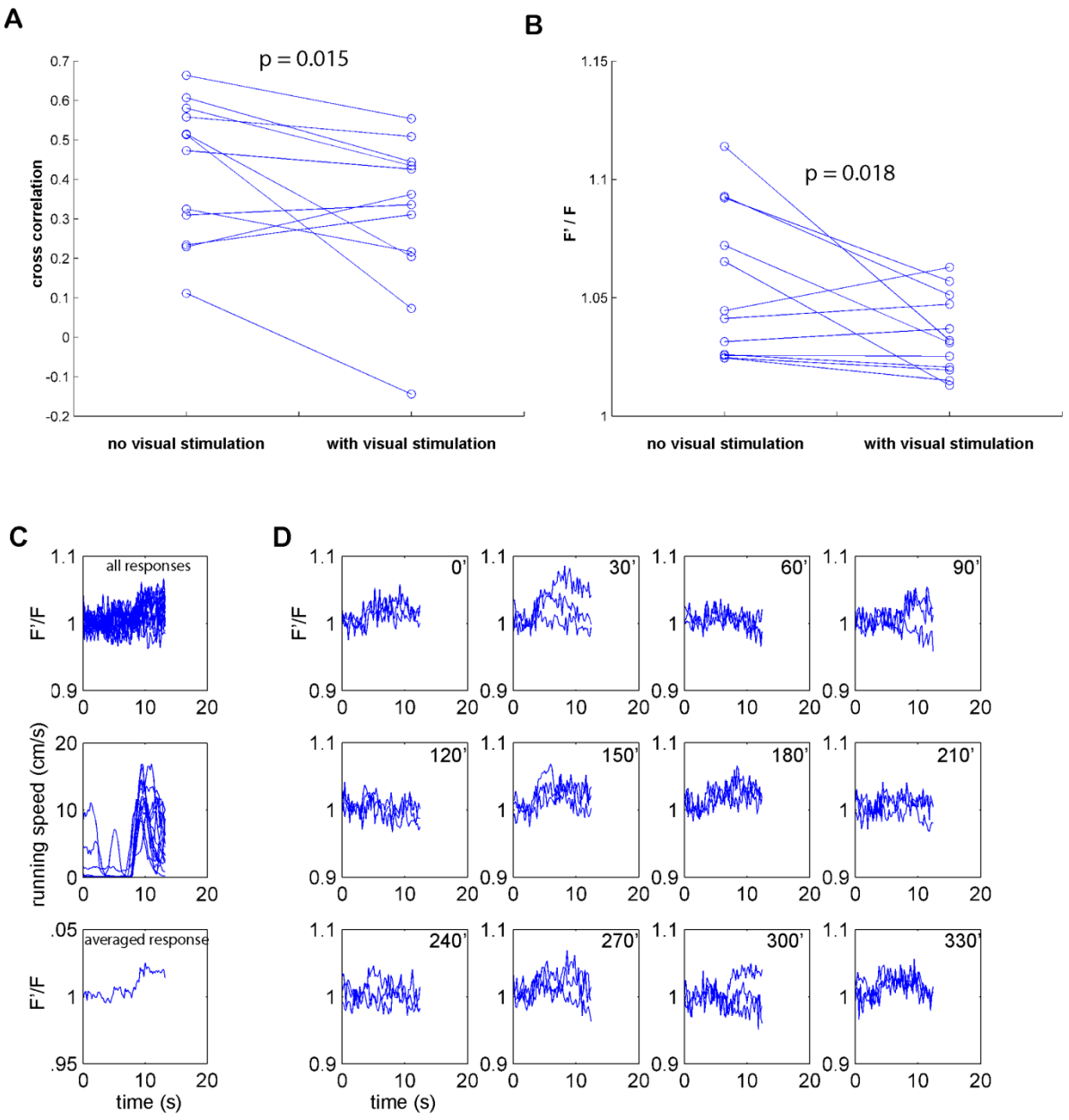

Supplemental Figure 2. Visual stimulation reduces locomotion-induced responses of VIP neurons, for the VIP neurons imaged with both visual stimulation and in darkness. Related to Figure 2. (A) Paired comparison of cross-correlation between calcium response and running speed for VIP neurons (n=12, 2 animals, paired Wilcoxon signed rank test). (B) Paired comparison between amplitudes of locomotion-induced calcium response of VIP neurons shown in (A) with and without visual stimulation (paired Wilcoxon signed rank test). (C-D) An example

of a VIP neuron's response to locomotion and visual stimulation in awake mouse. (C) Upper panel: all calcium responses aligned to onset of locomotion. Middle panel: all episodes of locomotion. Lower panel: Average calcium response of all the traces shown in upper panel. (D) Calcium response to the drifting gratings moving at different directions. Each blue trace is a single trial.

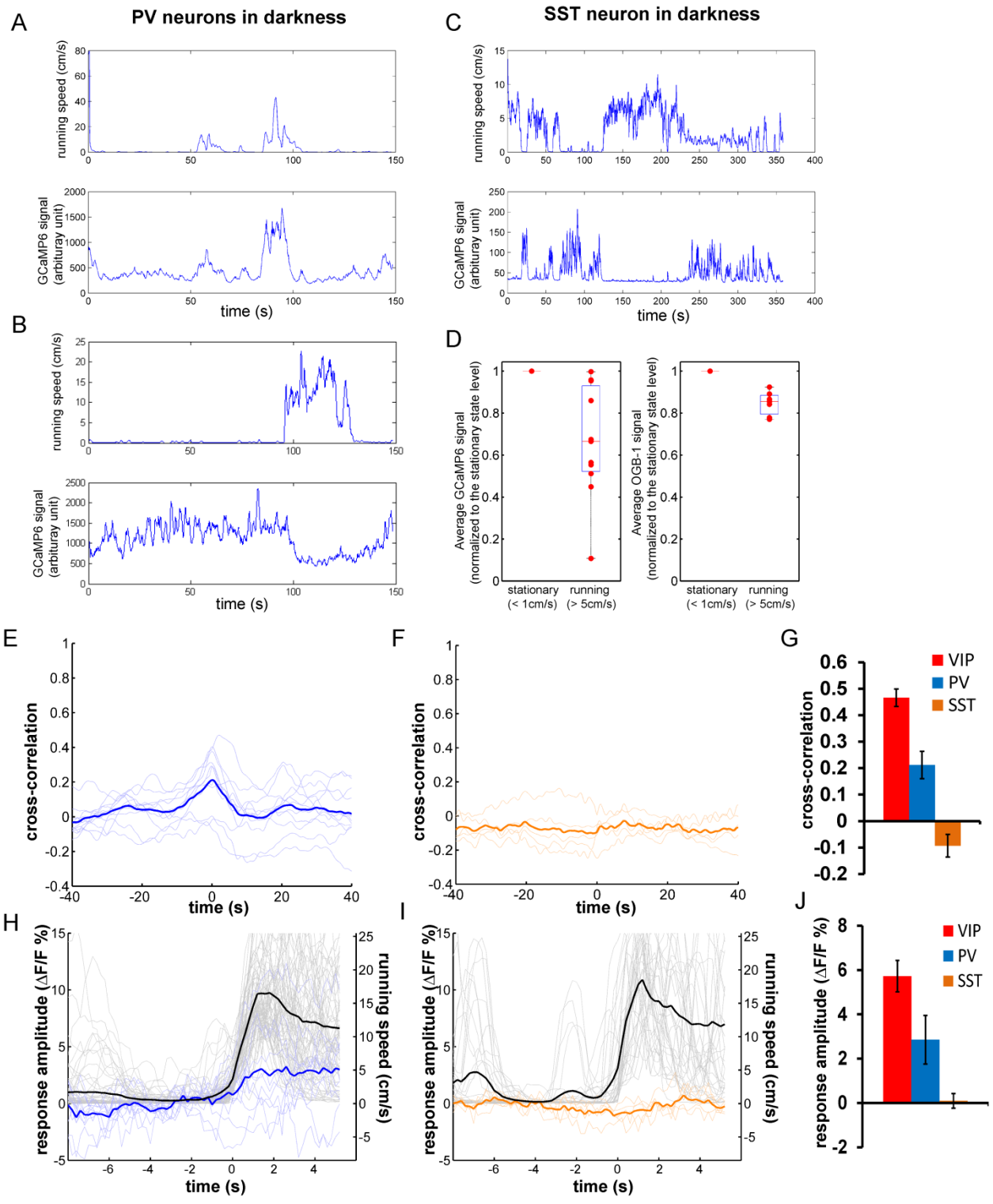

Supplemental Figure 3. Locomotion differentially modulates the responses of PV and SST neurons. Related to Figure 3. (A-B) Examples of calcium response of GCaMP6s expressing PV

neurons. PV neurons were labeled by injecting AAV-flex-GCaMP6 into PV-cre mice. (A) An example showing the activity of a PV neuron that was increased by locomotion. (B) An example showing the activity of PV neuron that was inhibited by locomotion. (C) An example of calcium response of GCaMP6s expressing SST neuron. SST neurons were labeled by injecting AAV-flex-GCaMP6 into SST-Cre mice. (D) The average calcium indicator fluorescent level of SST neurons during stationary and running states. For each neuron, baseline fluorescence (average of lower 5 percentile of all data points) was subtracted before normalizing the average fluorescent level during stationary state to 1 for comparison with the average fluorescent level during running state. Each red dot represents one neuron. Box-plot indicates the range of the value for all collected neurons. (E-J) Results from OGB-1 measurements. PV neurons were labeled by crossing PV-Cre and Ai14 mice. SST neurons were labeled by injecting AAV-DIO-TdTomato into SST-Cre mice. (E-F) The cross-correlation between the OGB-1 calcium signal and running speed for PV (E) and SST (F) neurons. The thin lines are the cross-correlation curves of all recorded neurons (A, n=11; B, n=5). The thick curve is the average of all thin curves. (G) The average zero-time cross-correlation for three types of inhibitory neurons (mean ±SEM). Value for VIP neurons from Figure 2A. (H-I) The calcium responses of PV (H) and SST (I) neurons are aligned to the start of running episodes (black traces). Thin traces (blue, orange or grey) show the average fluorescence and running speeds of all extracted events for each single neuron. (J) The average calcium response amplitude of three types of inhibitory neurons. The values are the average of the curves between 2s to 4s on the X-axis in (H-I). The value for VIP neurons was from Figure 2E.

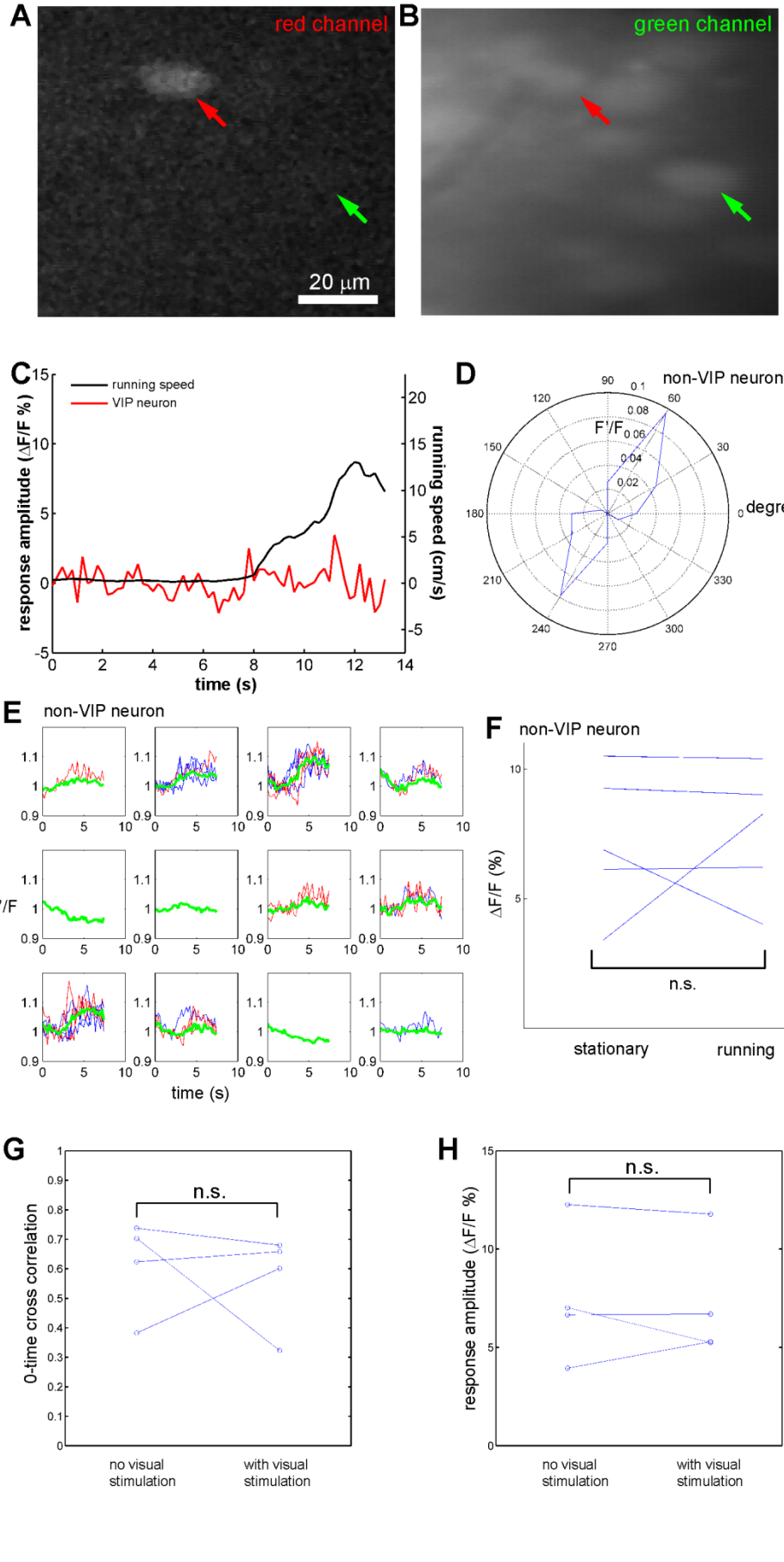
A
red channel
20 μm
B
green channel
C
running speed
VIP neuron
response amplitude (ΔF/F %)
running speed (cm/s)
time (s)
D
non-VIP neuron
F'/F
degree
E
non-VIP neuron
F'/F
time (s)
F
non-VIP neuron
ΔF/F (%)
n.s.
stationary
running
G
0-time cross correlation
n.s.
no visual stimulation
with visual stimulation
H
response amplitude (ΔF/F %)
n.s.
no visual stimulation
with visual stimulation

Supplemental Figure 4. Effect of local infusion of neurotransmitter antagonists. Related to Figure 4. (A-F) Local infusion of nicotinic antagonists MEC&MLA reduces response of VIP neurons to locomotion but does not abolish visual responses of non-VIP neurons. (A-B) After loading OGB-1, the images were taken at 910nm to visualize the TdTomato-expressing VIP neurons (A), and 800nm (B) to image the calcium response. Red arrows indicate VIP neuron; green arrows indicate non-VIP neuron. (C) The averaged calcium response of the VIP neuron in (A) to locomotion after nAChR blockade. (D) Polar chart and (E) fluorescence traces of visual response of the non-VIP neuron shown in (B) to gratings drifting in different directions after nAChR blockade (color conventions as in Supplemental Figure 1). (F) The response amplitudes after nAChR blockade were not different between stationary and running states for the non-VIP neuron shown in (B). (G-H) Local injection of glutamate receptor antagonist NBQX abolishes the influence of visual stimulation on the response of VIP neurons to locomotion. Paired comparison of the cross-correlation between calcium response and the running speed (G) and fluorescence response amplitude (H) of VIP neurons imaged with and without visual stimulation during NBQX application (n=4, paired Wilcoxon signed rank test) (compare with Supplemental Figure 2AB).

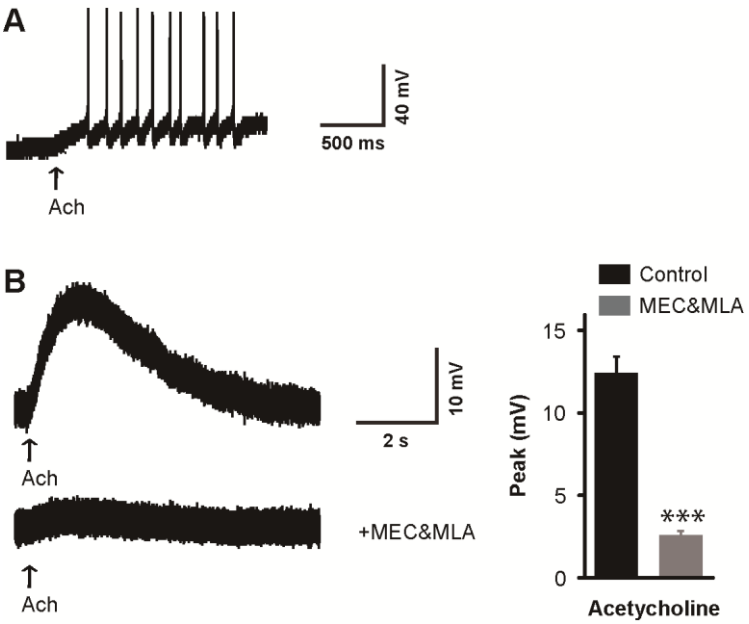

Supplemental Figure 5. VIP neurons are directly activated by ACh via nicotinic AChR. Related to Figure 4. (A) Whole-cell recording of a typical VIP neuron in visual cortex slice during puff application of acetylcholine (100 mM, 250 ms) in the absence of TTX in aCSF. VIP neuron fires action potentials immediately after ACh application. (B) Left, examples of acetylcholine responses before and after bath-application of mecamylamine (100 μM) and methyllycaconitine (0.1 μM). Right, all VIP neurons displayed acetylcholine responses (n=9), which were blocked in the presence of the nAChR antagonists (n=12). Values are mean ±s.e.m. (***P<0.01, Mann–Whitney U-test)

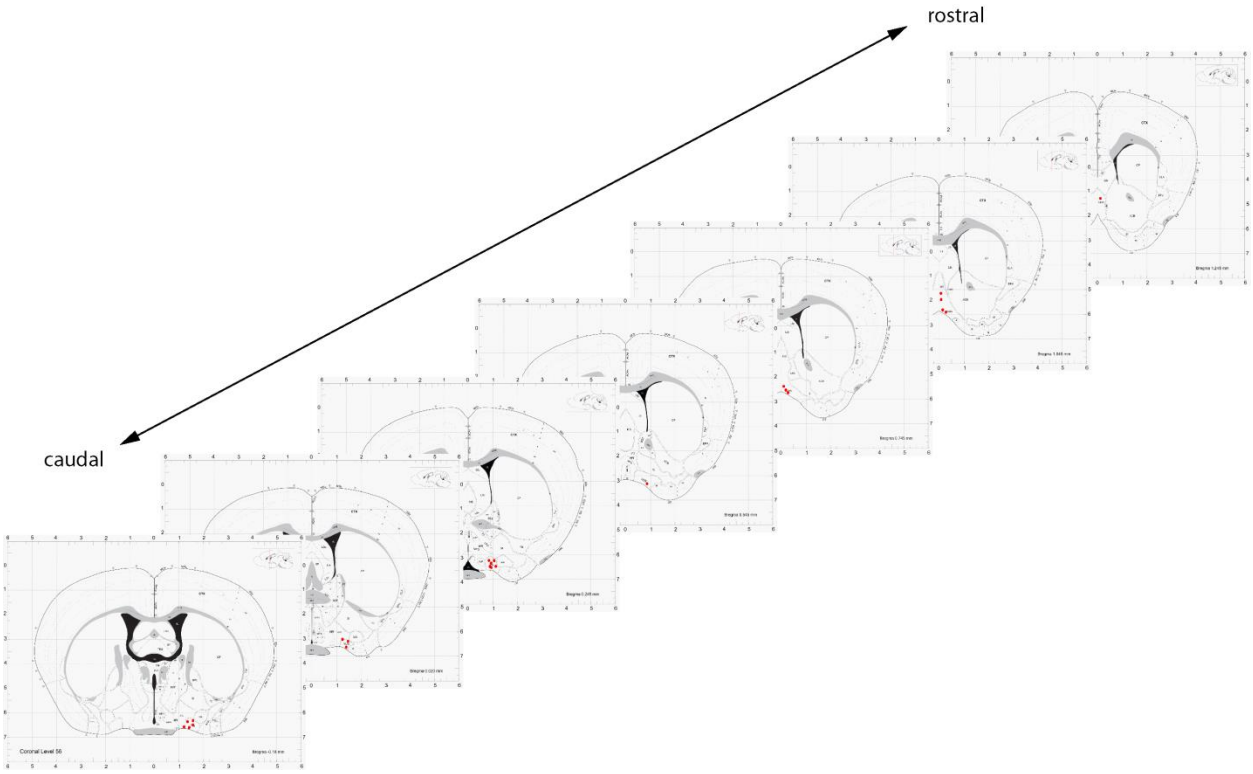

Supplemental Figure 6. Diagram of NBD neurons making monosynaptic connections with V1 superficial-layer VIP cells as identified by rabies virus mediated retrograde labeling. Related to Figure 5. Serial coronal sections showing locations of neurons in NDB labeled after rabies virus infection of V1 superficial-layer VIP neurons. Red dots represent the labeled neurons in a representative mouse.

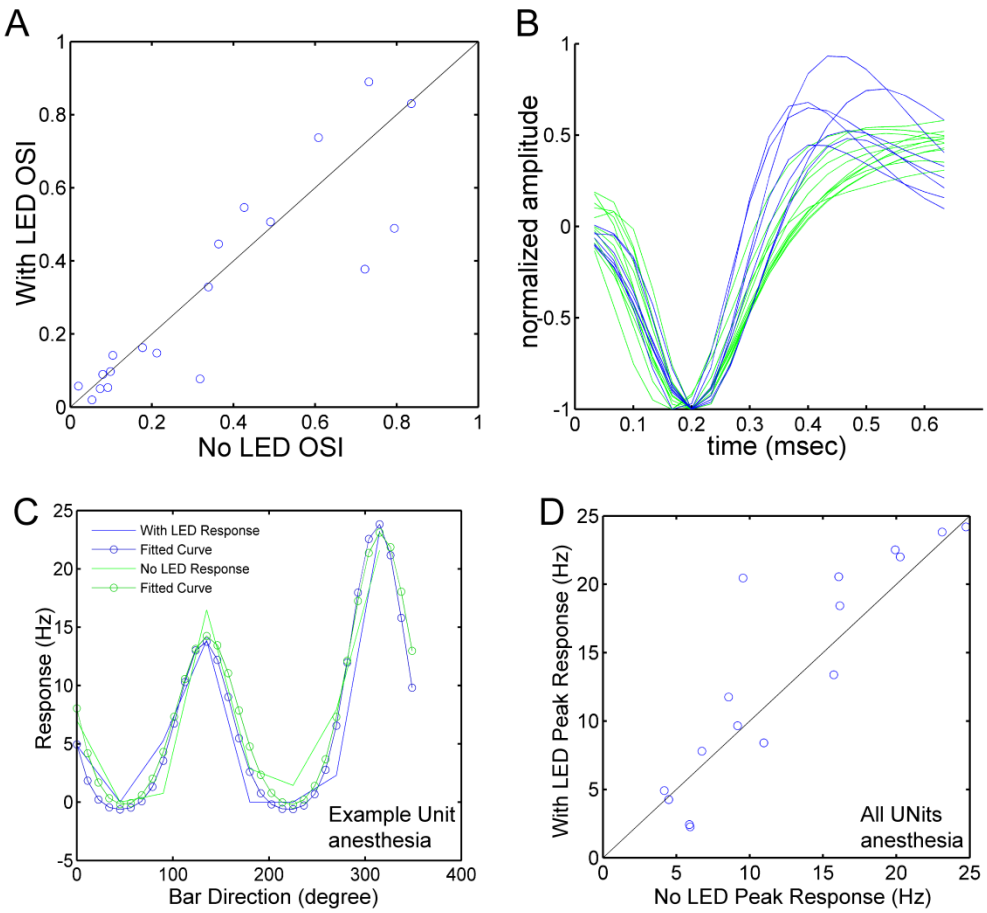

Supplemental Figure 7. Optogenetic activation of VIP neurons does not alter orientation selectivity in awake stationary animals and does not change the amplitude of visual responses in anesthetized animals. Related to Figure 6. (A) For the isolated unites shown in Figure 6D, the OSI did not change when the LED was turned on to activate VIP neurons. (B) The waveform of the broad spiking neurons (green) and the narrow spiking neurons (blue) from the isolated units shown in (A). (C) Orientation tuning of an isolated unit in control (No LED) condition and during optogenetic activation of VIP neurons (With LED) condition, in a VIP-Cre:Ai14 mouse injected with AAV-DIO-ChETA-YFP and anesthetized with 0.5mg/ml chlorprothixene and 0.75% isoflurane. The responses shown are the averages of 5 trials using moving bars, and the orientation tuning curves were fitted with double-Gaussian function. (D) Comparison of the peak

response values of isolated units in control (No LED) condition and during optogenetic activation of VIP neuron (With LED) condition, of anesthetized (0.5mg/ml chlorprothixene and 0.75% isoflurane) VIP-Cre:Ai14 mice injected with AAV-DIO-ChETA-YFP (blue circles, 15 units, 3 animals).

Supplemental Experimental Procedures:

Animal procedures

VIP-Cre (Taniguchi et al., 2011), PV-Cre, SST-Cre and ROSA-LNL-tTA (Wang et al., 2008) mice were from Jackson Lab, Ai14 mice were from Allan Brain Institute. Experiments were performed on adult (age 2-4 months) mice of either sex. The animals were maintained in the animal facility at University of California, San Francisco (UCSF) and used in accordance with protocols approved by the UCSF Institutional Animal Care and Use Committee. Animals were maintained on a 14hr light / 10hr dark cycle. Experiments were performed during the light phase of the cycle. For experiments described in Figure 5, animals were maintained in the animal facility at Cold Spring Harbor Laboratory (CSHL) and used in accordance with protocols approved by the CSHL's Institutional Animal Care and Use Committee.

Drugs

Acetylcholine, NBQX, mecamylamine (MEC) and methylycaconitine (MLA) are all from Sigma-Aldrich.

Preparation of mice animal for imaging on the spherical treadmill

Our spherical treadmill was modified from the design described in (Dombeck et a;l, 2007; Niell and Stryker, 2010). Briefly, a closed-cell foam ball (Plasteel Corporation) was placed on a base foam bowl with a single air inlet at the bottom. The base foam bowl was trimmed to allow the close placement of 2 USB-optical mice mouse for sensing the rotation of the floating styrofoam ball using custom driver software, which transmitted the USB signals to our data analysis system. The animal's head was fixed via a surgically attached steel headplate that could be screwed into a rigid crossbar above the floating ball.

For calcium imaging and tetrode recording in running mice, the custom stainless steel headplate with a 5-mm hole was cemented to the skull to allow head fixation. Animals were anesthetized with isoflurane in oxygen (3% induction, 1.5-2% maintenance) and given a subcutaneous injection of carprofen (5mg/kg) as a post-operative analgesic, and 0.2ml of saline to prevent post-operative dehydration. Following a scalp incision, the fascia was cleared from the surface of the skull, and a thin layer of cyanoacrylate (VetBond, WPI Inc.) was applied, to provide a substrate to which the dental acrylic could adhere. The metal headplate was then attached with dental acrylic, covering the entire skull except for the region in the center opening of the headplate, which was filled with a silicone elastomer (Kwik-Sil, WPI Inc.) to protect the skull. The animal was then allowed to recover. On the days following headplate attachment, the animal was allowed to habituate to the imaging setup, first by a period of handling by the experimenter, and then being allowed to stand on the surface of the ball. Finally, air pressure was applied to the ball and the headplate was screwed into the crossbar above the ball. For calcium imaging, the animal was allowed to run freely. For tetrode recording, whenever the animal began to run, the experimenter retarded rotation of the ball so that the animal could not run freely. After one or

two days of such practice, the animal generally remained stationary duirng visual stimulation, allowing us to collect data on visual responses without running.

Tetrode recording in awake mice

The recording was performed as described previously (Niell and Stryker, 2010) with little modification. On the day of recording, the animal was again anesthetized as described above. The silicone plug was removed, and the skull was thinned above the area of viral infection so that it was nearly transparent. A small opening in the skull was made with a 27 gauge needle to allow insertion of a 16 channel probe (Neuronexus model a2X2-tet-2mm-150-121). The electrode was placed at an angle of ~45deg relative to the cortical surface, to increase the distance between the insertion and recording sites and also place the electrodes closer to the center of the LED light path. The electrodes were inserted to a depth of <400um below the cortical surface to record cells in layer 2/3. For each animal, the electrode was inserted only once.

Visual stimulation, data acquisition, and analysis

Visual stimuli were presented as described previously (Niell and Stryker, 2008). Briefly, stimuli were generated in MatLab using the Psychophysics Toolbox extensions (Brainard, 1997; Pelli, 1997) and displayed with gamma correction on a monitor (Dell, 30X40cm, 60Hz refresh rate, 32cd/m^2 mean luminance) placed 25cm from the mouse, subtending ~60-75 ^{o}of visual space. For drifting bars, the spatial frequency was 0.2 cycles/deg (cpd), and the temporal frequency was 2Hz. For drifting sinusoidal gratings, the spatial frequency was 0.05 cpd and the temporal frequency was 2Hz. Stimulation was presented at nominal 100% contrast for 3sec with 3sec gray interval.

Data acquisition was performed as described by Niell and Stryker (Niell and Stryker, 2008). Signals were acquired using a System 3 workstation (Tucker-Davis Technologies) and analyzed with custom software in MatLab (MathWorks).

For single-unit activity, the extracellular signal was filtered from 0.7 to 7 kHz and sampled at 25 kHz. Spiking events were detected on-time by voltage threshold crossing, and a 1 ms waveform sample on all 4 recording surfaces of the tetrode was acquired around the time of threshold crossing. Single-unit clustering and spike waveform analysis was performed as described previously (Niell and Stryker, 2008), with a combination of custom MatLab programs and Klusta-Kwik (Harris et al., 2000). Quality of separation was determined based on the Mahalanobis distance and L-ratio (Schmitzer-Torbert et al., 2005) and evidence of clear refractory period. Units were also checked to assure that they responded similarly at the beginning and end of recording to ensure that they had not drifted or suffered mechanical damage. Typical recordings yielded 4-12 single units across the electrode, with 1-4 per tetrode group. As previously (Niell and Stryker, 2008), units were classified as narrow or broad spiking based on properties of their average waveforms, at the electrode site with largest amplitude.

For drifting gratings, responses at each orientation were calculated by averaging the spike rate during the 3s presentation and subtracting the spontaneous rate. For drifting bars, the response during the 3.75s presentation was fitted by a Gaussian curve and the peak was recorded as the response to that orientation. The preferred orientation was determined by averaging the response across all spatial frequencies, and calculating half the complex phase of the value $\sum F(\theta)e^{2i\theta} \Big/ \sum F(\theta)$. The orientation tuning curve was fitted as the sum of two Gaussians centered on θ_{pref} and $\theta_{pref} + \pi$, of different amplitudes A1 and A2 but equal width σ, with a

constant baseline B. The orientation selectivity index (OSI) (Kuhlman et al., 2011; Niell and Stryker, 2008) was calculated as $\sqrt{(\sum R(\theta_i) * \sin(2\theta_i))^2 + (\sum R(\theta_i) * \cos(\theta_i))^2} \Big/ \sum_i R(\theta_i)$.

AAV-flex-GCaMP6s, AAV-DIO-TdTomato and AAV-DIO-ChETA-YFP viral infection

Three to four weeks prior to headplate implantation, mice were injected stereotactically with AAV-2/5(or1)-CAG-flex-GCaMP6s, AAV-2/9-EF1a-DIO-ChETA-EYFP (UPenn Vector Core), or AAV-2/9-DIO-TdTomato (Josh Huang lab). Mice were anesthetized with isoflurane. A small bur hole was drilled into the skull using a dental drill over the primary visual cortex. A glass micropipette (tip size ~10-30um) attached to a Picospritzer was lowered below the pia surface to the specified coordinates. 0.5ul of the virus was injected with short pulses (50ms) over 5min. The glass pipette was left in place for an additional 3 min to allow viral diffusion. After removal of the injection pipette, the scalp was closed with cyanoacrylate and the animal allowed to recover for 3-4 weeks.

Photostimulation in vivo

One fiber-coupled blue LED (center wavelength 470nm, Thorlabs) was used to activate ChETA. The fiber was mounted on a manual manipulator and positioned less than 1mm from the craniotomy, as described in (Adesnik et al., 2012). LED light to activate ChETA was controlled using a Master8 triggered by our MatLab visual stimulation program. Each visual stimulation condition contained LED-on and LED-off conditions; different conditions were interleaved in random orderThe LED was driven at maximal current output from the LED driver.

Calcium imaging of genetically labeled neurons in awake, running mice

VIP, SST and PV positive neurons were labeled by crossing *Ai14* (Cre-dependent TdTomato expression) mice with *VIP-Cre, SST-Cre* and *PV-Cre* mice (Taniguchi 2012 Neuron), respectively. For calcium imaging, OGB-1 was loaded as described previously (Gandhi et al., 2008; Stosiek et al., 2003). Briefly, adult (2-4 month old) mice were anesthetized by inhalation of isoflurane. The primary visual cortex was identified by intrinsic signal imaging. The skull over the primary visual cortex was thinned and removed using stainless steel drill bits to make a craniotomy (~3mm). Immediately after removing the skull piece, the cortex was covered by cortex buffer (in mM: NaCl 125, KCl 5, Glucose 10, HEPES 10, MgSO4 2, CaCl2 2, PH 7.4). OGB-1 (50mg, Invitrogen) was dissolved in 4ul Pluronic F-127 (20% solution in DMSO, Invitrogen), 34ul loading buffer (in mM: NaCl 150, KCl 2.5, HEPES 10, PH 7.4) amd 2ul Alexa647. A micropipette was filled with this solution and inserted coaxially into the cortex. A pressure pulse (1min 10psi, Picospritzer II) was applied to the pipette to eject ~400fl of the dye-containing solution.

After dye loading, the craniotomy was covered by agrose and a round glass cover slip. The mouse was transferred to the trackball apparatus described above and was allowed to recover for ~40min before being imaged. The 2-photon imaging was performed using a Sutter Movable Objective Microscope and a Chameleon ultrafast laser, controlled by Scanimage. Images were taken at ~5Hz and the movement of the trackball was recorded as described previously (Niell and Stryker, 2010). The images were stabilized by aligning to a target image frame using an efficient cross-correlation-based registration algorithm (single-step discrete fourier transformation algorithm) (Guizar-Sicairos et al., 2008). The target image was obtained by mean projection of image frames from a trial visually identified to contain still frames. The stabilized images were then analyzed by ImageJ to get the time-series of calcium signal of selected region of interest.

The calcium signal trace was further analyzed by custom written MatLab program for aligment with the running episodes and with visual stimulation signals.

Rabies virus retrograde tracing and imaging

For rabies helper virus production, the AAV plasmid (AAV-TRE-HTG; Addgene plasmid 27437) (Miyamichi et al., 2011) was produced into AAV serotype 2/9 virus by the Virus Vector Core Facility of the University of North Carolina (Chapel Hill, NC). EnvA-pseudotyped, G-deleted virus (EnvA-SAD-ΔG-mcherry) had functional titers of 2×10^9 infectious units per milliliter and was purchased from the SALK Gene Transfer Targeting and Therapeutics Core (La Jolla, CA).

VIP-Cre and ROSA-LNL-tTA were maintained in C57BL/6 background and experiments were performed at 2-6 mo of age. Mice were anesthetized by i.p. injection of a ketamine/xylazine mixture (100mg/kg ketamine and 10mg/kg xylazine in sterile saline). Stereotactic injections were performed via rodent stereotax (David Kopf instruments model 900 series). A small bur hole was drilled into the skull using a dental drill (Henry Schein), over the primary visual cortex (AP, -4.00mm, ML, -2.75mm, DV, -0.45mm). A glass micropipette (tip size ~10-30μm) attached to a Picospritzer (General Valve) was lowered below the pia surface to the specified coordinates. 0.1-0.3μL of (1.6×10^{12} particles/ml) helper virus (AAV2/9-TRE-HTG) was injected. Two week later, 0.5 μL of rabies virus (EnvA-SAD-ΔG-mcherry) was injected under the same conditions in the same cortical area. 5-7 days post rabies infection mice were sacrificed.

Mice were intracardially perfused with PBS followed by 4% PFA in PBS. Following 24-48hrs of post fixation, coronal brain slices at 75 μm were sectioned using a vibratome. To demonstrate the GFP signal, chicken anti-GFP primary antibodies were used (1:1000, Aves Labs) followed by AlexaFluor488 goat anti-chicken secondary antibody (1:500, Molecular Probes). Rabbit

polyclonal anti-RFP antibody (1:1000, Rockland) was used with AlexaFluor594 goat anti-rabbit secondary antibody (1:500, Molecular Probes) to demonstrate the mCherry signal. Sections were counterstained with NeuroTrace Nissl Stain (Molecular Probes). Images were acquired with a Zeiss 710 LSM confocal microscope and images were viewed using ImageJ. Anatomical regions were identified using the Paxinos and Allen Institute Mouse Brain Atlases.

In vivo drug injection

After making craniotomy and loading OGB-1, the animal was quickly transferred to the 2-photon imaging setup. A glass pipette with an opening 20-40μm loaded with different channel blockers or loading buffer and Alexa-594 solution was inserted to the cortical area loaded with OGB-1 under the guidance of 2-photon imaging, while the animal was still under anesthesia using 2% isoflurane. The glass pipette was controlled by Nanoject-II (Drummond Scientific), and the solution was injected manually at 4.6nl per injection. After placing the pipette in the proper position in the fluid above the brain, a few test injections were made to insure the pipette was not blocked. Care was taken to avoid blood vessels. After inserting the pipette, the craniotomy was covered by agrose and a round glass cover slip, which was further sealed by crazy glue and dental acrylic. The animal was then allowed to recover on the trackball. After fully recover from anesthesia (~45min), drug was injected at a rate of 4.6nl per injection per second for 110 times. The imaging was performed 5min after injection and continued no longer than 25min after injection.

Electrophysiological recording in vitro and local puffing

Coronal sections (300-μm thick) of visual cortex were prepared from VIP-Cre::Ai14 mice (>8 weeks old) using a Microslicer DTK-Zero1 (Ted Pella) in chilled high sucrose cutting solution

containing (in mM): 2.5 KCl, 7 $MgSO_4$, 1.25 NaH_2PO_4, 25 $NaHCO_3$, 7 glucose, 210 sucrose, 1.3 ascorbic acid (95%O_2/5% CO_2). The slices were then incubated for 30 min at 34 ℃ in artificial cerebral spinal fluid (aCSF) containing (in mM): 119 NaCl, 2.5 KCl, 1 NaH_2PO_4, 26.2 $NaHCO_3$ and 11 glucose, 2.5mM$CaCl_2$ and 1.3mM$MgSO_4$. The aCSF was bubbled with 95%O_2 and 5% CO_2 to maintain pH, and the acute slices were allowed to recover at room temperature for 45 min to 1 h. During recording, slices were transferred to a perfusion stage on an Olympus BX51WI upright microscope and perfused at 2.5 ml/min with aCSF containing 0.1mM picrotoxin. Whole-cell current-clamp recordings were performed with patch pipettes (4–6 MΩ resistance) filled with intracellular solution containing (in mM): 140 K-gluconate, 10 HEPES, 7 NaCl, 4 Mg-ATP and 0.3 Na-GTP (290 mOsm and pH 7.3 with KOH). Data were gathered through a MultiClamp 700B amplifier (Axon Instruments), filtered at 2 kHz, and digitized at 10 kHz. Signals were analyzed using Igor Pro (Wavemetrics). The VIP neurons were identified with RFP fluorescence. Local puff application of Acetylcholine (100 mM, 200–300 ms duration) was delivered from a patch pipette connected to a picospritzer (Parker Hannifin Corporation).

Photolytic damage of VIP neurons *in vivo*

Images were taken under 910nm to identify appropriate VIP neurons to photo damage. After being selected, laser scanning area was zoomed in to scan the cell body of selected neurons. The laser power was then increased and the zoomed in area was scanned continuously for 30sec. We ablated 5-10 neurons in a less than 200X200 μm^2 area

References for supplemental information:

Adesnik, H., Bruns, W., Taniguchi, H., Huang, Z.J., and Scanziani, M. (2012). A neural circuit for spatial summation in visual cortex. Nature *490*, 226-231.

Brainard, D.H. (1997). The Psychophysics Toolbox. Spat Vis *10*, 433-436.

Gandhi, S.P., Yanagawa, Y., and Stryker, M.P. (2008). Delayed plasticity of inhibitory neurons in developing visual cortex. Proc Natl Acad Sci U S A *105*, 16797-16802.

Guizar-Sicairos, M., Thurman, S.T., and Fienup, J.R. (2008). Efficient subpixel image registration algorithms. Opt Lett *33*, 156-158.

Harris, K.D., Henze, D.A., Csicsvari, J., Hirase, H., and Buzsaki, G. (2000). Accuracy of tetrode spike separation as determined by simultaneous intracellular and extracellular measurements. J Neurophysiol *84*, 401-414.

Kuhlman, S.J., Tring, E., and Trachtenberg, J.T. (2011). Fast-spiking interneurons have an initial orientation bias that is lost with vision. Nat Neurosci *14*, 1121-1123.

Miyamichi, K., Amat, F., Moussavi, F., Wang, C., Wickersham, I., Wall, N.R., Taniguchi, H., Tasic, B., Huang, Z.J., He, Z., *et al.* (2011). Cortical representations of olfactory input by trans-synaptic tracing. Nature *472*, 191-196.

Niell, C.M., and Stryker, M.P. (2008). Highly selective receptive fields in mouse visual cortex. J Neurosci *28*, 7520-7536.

Niell, C.M., and Stryker, M.P. (2010). Modulation of visual responses by behavioral state in mouse visual cortex. Neuron *65*, 472-479.

Pelli, D.G. (1997). The VideoToolbox software for visual psychophysics: transforming numbers into movies. Spat Vis *10*, 437-442.

Schmitzer-Torbert, N., Jackson, J., Henze, D., Harris, K., and Redish, A.D. (2005). Quantitative measures of cluster quality for use in extracellular recordings. Neuroscience *131*, 1-11.

Stosiek, C., Garaschuk, O., Holthoff, K., and Konnerth, A. (2003). In vivo two-photon calcium imaging of neuronal networks. Proc Natl Acad Sci U S A *100*, 7319-7324.

Taniguchi, H., He, M., Wu, P., Kim, S., Paik, R., Sugino, K., Kvitsiani, D., Fu, Y., Lu, J., Lin, Y., *et al.* (2011). A resource of Cre driver lines for genetic targeting of GABAergic neurons in cerebral cortex. Neuron *71*, 995-1013.

Wang, L., Sharma, K., Deng, H.X., Siddique, T., Grisotti, G., Liu, E., and Roos, R.P. (2008). Restricted expression of mutant SOD1 in spinal motor neurons and interneurons induces motor neuron pathology. Neurobiol Dis *29*, 400-408.